Official journal of the JHL 2689-9620
www.light-am.com

Review Open Access

Two-photon lithography for integrated photonic packaging

Shaoliang Yu[1,*], Qingyang Du[1,*], Cleber Renato Mendonca[2,3], Luigi Ranno[2], Tian Gu[2,4] and Juejun Hu[2,4]

Abstract

Photonic integrated circuits (PICs) have long been considered as disruptive platforms that revolutionize optics. Building on the mature industrial foundry infrastructure for electronic integrated circuit fabrication, the manufacturing of PICs has made remarkable progress. However, the packaging of PICs has often become a major barrier impeding their scalable deployment owing to their tight optical alignment tolerance, and hence, the requirement for specialty packaging instruments. Two-photon lithography (TPL), a laser direct-write three-dimensional (3-D) patterning technique with deep subwavelength resolution, has emerged as a promising solution for integrated photonics packaging. This study provides an overview of the technology, emphasizing the latest advances in TPL-enabled packaging schemes and their prospects for adoption in the mainstream photonic industry.

Keywords: Photonic packaging, Two-photon lithography, Photonic wire bonding, Microoptics, Integrated photonics

Introduction

Photonic integrated circuits (PICs), which involve the dense integration of optical components and systems on planar substrates[1–4], have been widely applied in communications[5], ranging[6], sensing[7], computing[8], spectroscopy[9], and quantum technology[10]. The scalable manufacturing of PICs is now an industry norm that leverages mature semiconductor-fabrication technologies derived from electronic integrated circuit (EIC) processing to reduce costs while enhancing performance[11,12].

Photonic packaging presents a different perspective. Compared with electronic packaging, the packaging of PICs demands a much higher alignment accuracy owing to the strict matching conditions for optical modes[13–15]. The alignment tolerance of optical interfaces is typically at the micron or even submicron level, which is one order of magnitude smaller than that of solder bump connections in electronic assemblies[16–18]. The tight alignment tolerance of PICs makes them incompatible with mainstream electronic packaging techniques and infrastructure, precluding cost reduction by exploiting economies of scale. Moreover, the heterogeneous or hybrid integration of multiple material platforms, such as silicon III-V, and lithium niobite, is increasingly in demand to fulfill new functionalities that Si-based materials alone cannot offer. The ability to accommodate advanced heterogeneous or hybrid integrated platforms is another obstacle in photonic packaging. New packaging technologies and device architectures are required to address these challenges[19–22].

Two-photon lithography (TPL) is an emerging approach that has received significant attention in recent years[23,24]. TPL is a laser direct-writing technology capable of carving

Correspondence: Shaoliang Yu (yusl@zhejianglab.com) or Qingyang Du (qydu@zhejianglab.edu.cn)
[1]Zhejiang Laboratory, Hangzhou 311100, China
[2]Department of Materials Science and Engineering, Massachusetts Institute of Technology, Cambridge, MA 02139, USA
Full list of author information is available at the end of the article.

© The Author(s) 2023
Open Access This article is licensed under a Creative Commons Attribution 4.0 International License, which permits use, sharing, adaptation, distribution and reproduction in any medium or format, as long as you give appropriate credit to the original author(s) and the source, provide a link to the Creative Commons license, and indicate if changes were made. The images or other third party material in this article are included in the article′s Creative Commons license, unless indicated otherwise in a credit line to the material. If material is not included in the article′s Creative Commons license and your intended use is not permitted by statutory regulation or exceeds the permitted use, you will need to obtain permission directly from the copyright holder. To view a copy of this license, visit http://creativecommons.org/licenses/by/4.0/.

almost arbitrary 3-D structures with resolutions well below the classical diffraction limit[24]; it was first reported in 1997[25], and has since been adapted to form on-demand optical connections[26–34]. TPL offers several unique advantages for photonic packaging[35].

1) In integrated photonics, light guiding can occur in various material platforms, such as silicon, glasses, III-V semiconductors, lithium niobate, and polymers, with significant differences in mode size and profile. TPL is uniquely suited for constructing broadband 3-D photonic structures with numerous geometric degrees of freedom to facilitate on-demand beam shaping and mode transformation between different waveguide systems. This is critical for achieving high coupling efficiency with wide bandwidths when connecting different optical components in a system (e.g., from lasers to single-mode waveguides).

2) TPL can be used to form optical connections between photonic components after assembly because the shape of the connections can be customized according to the relative displacement between the components. This approach significantly relaxes the alignment tolerance during PIC assembly and enables the utilization of standard electronic assembly techniques such as pick-and-place.

3) TPL can create high-channel-density, low-loss 2.5-D or 3-D links to accommodate the height differences between the optical ports inside a package. This is particularly important for hybrid integration in which modules are patterned on different substrates with varying thicknesses. This feature relaxes the accuracy and uniformity requirements during wafer lapping and deep trench etching[36–38]. Commonly used TPL resins exhibit broadband low optical attenuation, making them suitable for building low-loss optical links between dissimilar material platforms.

4) In addition to creating optical links, TPL can be used to form micro- and nano-mechanical structures to guide precise component placement in a passive alignment process or in pluggable optical connectors.

In this study, we present a comprehensive overview of the latest advances in TPL technology for integrated photonic packaging. Fig. 1 shows schematics highlighting these packaging methods. The basic principles of TPL are briefly introduced, followed by a survey of TPL-based photonic packaging methods. We then focus on their commercial implementation in the photonics industry and conclude by discussing of future research directions.

Basic Principles of TPL

Working principle and printing systems

TPL is a 3-D printing technology that leverages a focused laser beam to selectively solidify a liquid photopolymer. The focused laser light causes two-photon polymerization (TPP) of the photoresist, leading to a solid structure. Unlike single-photon lithography, TPP occurs when the laser intensity exceeds a certain threshold value at the laser focal spot. Thus, TPL enables a more controlled and localized polymerization process, which results in finer resolution and higher precision.

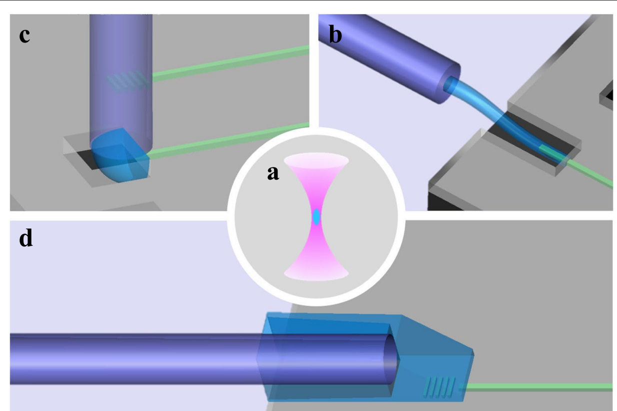

Fig. 1 Schematic drawings of three typical packaging methods based on TPL. **a** Illustration of a TPL voxel located at the focal spot of a laser beam. The focal spot is translated through the volume of the resin to enable direct writing of 3-D structures. **b** Photonic wire bond. **c** Freeform microoptics. **d** Mechanical alignment structure.

A schematic of a typical TPL printing system is shown in Fig. 2. The laser, operating in the near-infrared region, is focused onto the sample by the objective lens, delivering a high light intensity that is absorbed by the photoinitiator present in the photoresist via two-photon absorption. To select a suitable magnification for the lens, the writing speed must be balanced with the desired resolution. A higher magnification yields a finer structural resolution, but results in a significantly reduced writing speed. A confocal imaging system helps locate the sample surface and enhances alignment accuracy. The galvo scanner and sample stage define distinct writing schemes, which are

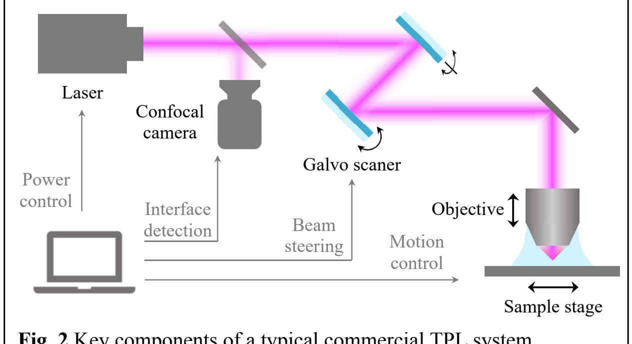

Fig. 2 Key components of a typical commercial TPL system.

discussed in Section 2.3. All components are connected to a computer for remote control and programming. Before printing, the software prompts a user interface that enables the operator to input the desired 3-D model and set printing parameters such as layer thickness and laser intensity. Full automation of such printing systems endows the TPL tool with a complex and highly precise system that enables the creation of intricate, high-resolution 3-D structures for a wide range of applications.

Material systems

The immense power of TPL to unlock the third dimension has enabled researchers to fabricate a variety of functional structures with exceptional performances in disparate applications, ranging from optics[39–41] to biomedicine[42–47]. The simple operation mechanism of TPP enables a wide range of material classes to be used, which further adds to the value offered by this technique.

The most mature family of chemicals used as the basis for TPP resins is acrylates (Fig. 3a), and a variety of commercial formulations specially designed for TPP[48] are already available. Polymer chains are formed through a free-radical polymerization process[44] that is compatible with a variety of photoinitiators. These polymers reach extremely high printing resolutions[49] and excellent optical[50] and mechanical properties[51,52]. Some examples of resins belonging to this polymer class include the series of “IP” resists, commercially available from Nanoscribe GmbH, or “Up” resists, available from UpNano GmbH. For instance, IP-Dip, one of the most commonly used members of the IP family of resins, is a photoresist designed for TPL to achieve the highest resolution. IP-Dip’s chemical composition is approximately $CH_2N_{0.001}O_{0.34}$, with the majority of the volume (60%–80%) being pentaerythritol triacrylate (PETA)[48]. IP-Dip is an index matched with immersion oil, for which high numerical aperture objectives are used to reduce structural distortions. This has enabled researchers to demonstrate the accurate printing of sub-100-nm features through sub-threshold resist exposure[53] or controlled heat treatment-induced shrinkage[54].

Other notable members of the IP family of resins include IP-n162, a resist designed for microoptics that boasts a high refractive index[55], and IP-S, which features a low degree of shrinkage in tandem with a smooth surface finish[56]. These photoresists have been used extensively in the production of microoptical devices, including reflective elements for coupling light into an optical fiber[57,58] or refractive/diffractive microlenses[40,41,59] (Fig. 3b). UpNano’s UpBlack and Nanoscribe’s IP-Black are two more formulations of particular interest in optics, as they enable the design of novel optics where not only the path of light is controlled through transparent refractive elements but also by modulating the intensity with absorptive elements[39]. For instance, Schmid et al. demonstrated the benefits of combining transparent and opaque structures fabricated via TPP to form microoptical elements with vastly improved contrast, such as a pinhole camera or telecentric lens with a custom 3-D aperture, with vastly improved contrast[39]. Another technologically relevant photoresin is UpThermo, a resist developed in collaboration with UpNano and Cubicure for hot lithography[60]. The increased thermal stability of UpThermo provides an obvious advantage over other photoresins for situations in which printed structures must undergo thermal processes after printing and development. This feature makes it an intriguing alternative to backend-of-the-line solutions for electronic/photonic packaging, which requires elevated temperatures for solder reflow or eutectic bonding[13].

Siloxanes are another family of resists extensively used in industry and academia. These chemicals have a polymeric backbone composed of alternating silicon and oxygen atoms (Fig. 3a) and can perform free radical or cationic polymerization[48]. The most prevalent photoresist belonging to this family is polydimethylsiloxane (PDMS), which is available from Nanoscribe in the form of IP-PDMS, as a formulation tailored for TPL, as well as from other vendors. This resist has been used for a range of applications in life sciences and microfluidics[61,62] owing to its non-cytotoxicity, flexibility, ease of functionalization, and optical transparency[63].

Another family of polymers that is relevant is epoxies (Fig. 3a), which have already become the material of choice for various applications owing to their excellent properties as adhesives[64] and coatings[65]. Although epoxy-based formulations are not as common as acrylates in TPL because of their requirements for thermal postprocessing to achieve complete polymerization of the printed structures, their lower shrinkage[66] gives them a key advantage for the printing of structures with critical size requirements. The chemical backbone of epoxies is composed of carbon and oxygen, which are formed upon cationic polymerization by opening the epoxide ring[44]. The most common epoxy-based TPL formulation is SU-8, which has been successfully used to fabricate high-aspect-ratio structures[67], microswimmers[68], and microfluidic channels[69].

Finally, a wide variety of organic-inorganic hybrid polymers has been proposed as potential TPL photoresists. A famous family of these compounds is organoceramics, most famously Microresist Technology GmbH’s ORMOCERs (organic modified CERamics). Their chemical structure is composed of a Si-O polymeric

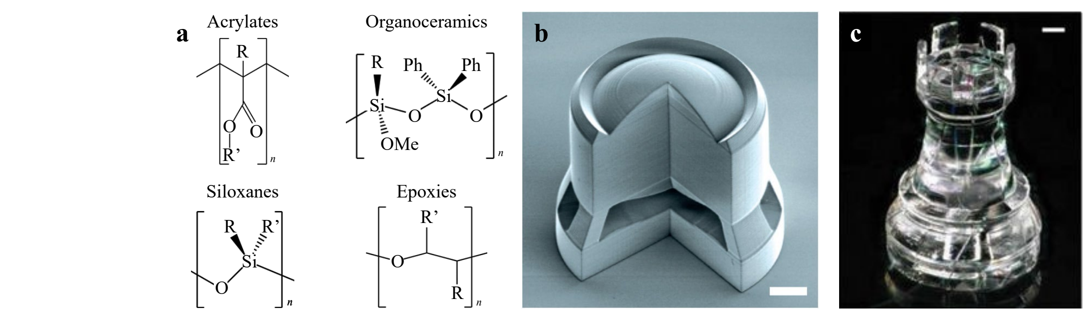

Fig. 3 Resin for TPL. **a** Polymeric backbone for some common TPP resins. In the chemical structure of organoceramic polymers, Me and Ph stand for methoxy and phenol groups, respectively. **b** Scanning electron micrograph of a doublet compound lens made of an IP-S acrylate-based photoresist. Reprinted from Gissibl et al.[93]. Scale bar, 20 µm. **c** Fused silica micro-rook fabricated through the debinding and sintering of a printed GP-Silica structure. Scale bar, 200 µm. Reprinted from Kotz, et al.[74].

backbone (Fig. 3a), with side groups determining the final properties of the polymer[70]. The most well-known member of the ORMOCER family is OrmoComp, a hybrid organic-inorganic photoresist with the molecular formula $C_{21}SO_8SiH_{36}$[48]. OrmoComp has low optical absorption from infrared to near-UV[55] as well as high printing resolution[71] and thermal stability[48], making this photoresin have potential applications in optics and related fields[72].

SZ2080 is another hybrid organic-inorganic sol-gel photoresin manufactured by IESL-FORTH with the chemical formula $C_4H_{12}SiZrO_2$[48], and its structure is similar to that of OrmoComp, except that the silicon atoms are substituted with zirconium atoms[48]. Recently, it was reported that the full conversion of SZ2080 into a completely inorganic material can be achieved by calcination of the printed structures at 1100 °C[73].

A similar approach to the calcination of SZ2080 was used to demonstrate a resin capable of printing glass, Nanoscribe GP-Silica[74]. This photoresin is based on a methacrylate/acrylate polymeric backbone with dispersed fused silica particles of ~40 nm diameter[74]. This has evolved from applications in mold casting[75] and later 3-D stereolithography printing[76] to high-resolution and commercially available TPL resists. The printed structures can be converted into transparent glass parts through a two-step process consisting of a debinding step at 600 °C to remove the organic component (which results in a highly porous structure) and a sintering step at 1300 °C to fuse the particles together[74], yielding a transparent part with optical properties comparable to those of fused silica, as shown in Fig. 3c. The structures exhibited considerable shrinkage, in excess of 25%, which could be used to produce parts smaller than the resolution limit of the printing process[74].

The embedding of nanoparticles within two-photon resins to produce composite structures is not limited to fused silica; a large variety of materials have already been demonstrated. This process adds one more dimension to tune the final properties of printed structures by imparting functions that polymeric materials normally lack, for example, a large refractive index, high thermal conductivity, or high magnetic response. Suter et al.[77] fabricated microswimmers that could be controlled through the application of an external magnetic field by embedding magnetite nanoparticles (~11 nm diameter) in SU-8. Masui et al.[78] fabricated methyl methacrylate (MMA) structures with a dispersion of Au nanorods for application in plasmonics. Similarly, Marino et al.[79] doped OrmoComp with barium titanate nanoparticles to create piezoelectric scaffolds for cell stimulation[34,35].

Another family of materials that has sparked the interest of the scientific community is hydrogels, that is, materials composed of a polymeric solid network with interstitial fluids. Hydrogels have shown many promising applications in the biomedical fields and life sciences[80], for example, as scaffolds for cells[81]. Hydrogels designed for life sciences are already commercially available; for example, BIO INX. In addition to their vast array of biological applications, hydrogels have also been used as a medium for embedding other materials[82,83], enabling the fabrication of 3-D structures with novel optical properties. For instance, the inclusion of cobalt-doped titanium oxide (CTO) into hydrogels has been reported to enable the fabrication of structures with large transparency windows all the way down into the UV and tunable birefringence upon the application of a weak magnetic field, enabling the facile modulation of light with promising applications in photonic packaging, flexible optics, and broadband anisotropic optical elements[82,83].

In the context of functional materials, much work has been done toward the realization of solid metallic or ceramic components through TPP to reduce the critical dimensions that can be commonly achieved through

additive manufacturing[82]. For instance, Vyatskikh et al.[46] used a custom nickel-acrylate resin to produce solid nickel parts upon pyrolysis and H_2 reduction of the metal. A similar approach was adopted by Luitz et al.[46], who engineered a platinum-containing organic-inorganic hybrid resin to fabricate solid metallic parts after a debinding process and full reduction of platinum salts. Other research groups[84,85] used hydrogels to achieve similar results. Sol–gelFor the case of ceramics, sol-gel templates that can be preferentially polymerized using a two-photon process have been investigated for use in ceramics[86].

In addition to inducing the localized polymerization of a photoresist, TPL has also been used to successfully pattern other material systems in three dimensions, most notably chalcogenide glasses[87–90] and metal–organic frameworks[91,92]. Wong et al.[88] fabricated a 3-D woodpile photonic crystal using As_2S_3. The chalcogenide glass was deposited at a high rate and low temperature, yielding an initial structure rich in As_4S_6 cages, which could then be converted back into a stable As_2S_3 network, enabling the selective removal of leftover material via wet etching. Similarly, Yu et al.[92] identified a metal organic framework whose fluorescence could be spatially modulated by direct laser writing (as a two-photon process) or direct UV irradiation.

In conclusion, the large library of materials compatible with direct laser writing enables designers to produce structures with finely tuned 3-D geometry as well as physical properties. We predict that in the coming years, as customized resins and novel active materials will be developed, TPL will become increasingly relevant as a manufacturing technology capable of bridging the gap between macroscale additive manufacturing and 3-D high-resolution lithography.

Writing schemes

In contrast to one-photon lithography, in which exposure is applied to a 2-D plane, the polymerization reaction of TPL only appears at the focal point with a high optical intensity. Thus, the voxelization of a geometry followed by point-by-point exposure is an essential procedure for the construction of 3-D photonic structures, resulting in a tradeoff between surface quality and throughput[98]. A finer slicing and hatching distance or higher voxel overlap benefits surface smoothness and shape accuracy, but burdens the writing speed. Conversely, a coarse mesh introduces a step effect[99] and degrades the surface quality, which can exacerbate optical scattering and loss in photonic applications.

Several slicing strategies have been proposed to overcome step effects, particularly for curved surfaces[98]. Instead of uniform slicing and hatching (Fig. 4a), annular scanning[100,101] and equal-arc scanning[102] modes are two representative slicing schemes that can achieve a much smoother surface (Fig. 4b). The slicing thickness was dynamically changed by considering the slope of curvature to mitigate the surface roughness and shape error. Furthermore, a smart slicing strategy of dynamically adjusting the voxel size simultaneously (Fig. 4c) can help obtain a better fit of the curvature without increasing the number of layers. Roughness down to 14 nm was achieved on a non-spherical microstructure with planar facets and relatively sharp edges and corners, simultaneously showing 3- and 5-fold reductions in roughness and throughput, respectively[103].

Table 1 Properties of resins for TPL.

Resin	Composition	n (λ = 780 nm)	E (GPa)	Density (g/cm3)	Viscosity at 20 °C (mPas)	Remarks
IP-Dip	Acrylate (PETA)	1.54[55]	0.75–2.5[94]	1.17	2420	High Resolution
IP-S	Acrylate	~1.49[50]	2.1	1.11	13600	Smooth surfaces
IP-Visio	Acrylate	~1.50[55]	0.17 ± 0.15[95]	–	–	Non-cytotoxic, low fluorescence
IP-n162	Acrylate	~1.61[55]	–	–	–	High refractive index
PDMS	Siloxane, $CH_3NSi(CH_3)_3$	~1.4[96]	~0.015	1.01	~100	Soft, non-cytotoxic
OrmoComp	Organoceramic	~1.51[55]	~1	~1	2000	Low absorption down to violet
SU-8	Epoxy	~1.56	~4[65]	~1.1	~12000	Low shrinkage, well established
GP-Silica	SiO2 (After post-processing)	~1.45[97]	68.3	–	–	Glass part after post-processing

Note: n, refractive index; λ, wavelength; E, Young's modulus. Data without marked references are quoted from the vendor.

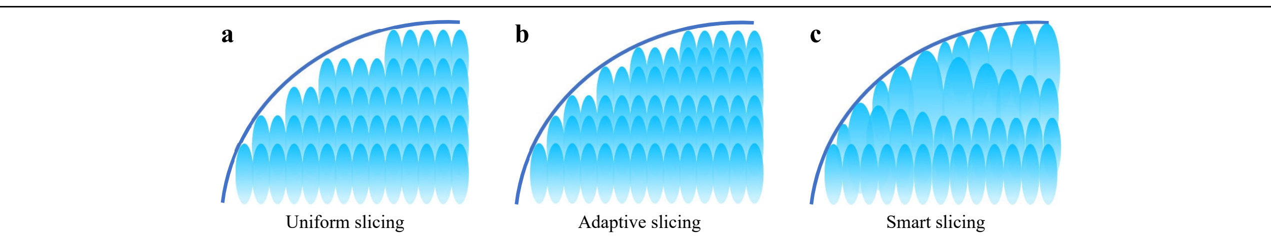

Fig. 4 Slicing strategies of TPL. **a** Uniform slicing with equal slicing height and hatching distance. **b** Adaptive slicing with changeable slicing thicknesses. **c** Smart slicing with dynamically changing slicing distances and voxel sizes.

In addition to the slicing scheme, there are other approaches for improving the surface quality and throughput[104]. Drawing upon super-resolution imaging methods, the resolution can be improved by stimulated emission depletion (STED) lithography[105] and peripheral photoinhibition (PPI) lithography[106]. A voxel size of 36 nm can be achieved by mitigating the systematic chromatic aberration[107] far beyond the diffractive limit. The profile/contour-scanning mode is another approach for mitigating roughness by tracing the outer contour profiles of structures in 3-D space[108]. Its combination with the flood exposure of the inner core is a promising strategy for improving both surface quality and throughput. Thermal reflow is also an efficient method for reducing the surface roughness of TPL-defined structures[109].

TPL-Based Photonic Packaging Methods

Photonic wire bond (PWB)

The concept of photonic wire bonding was first introduced at Karlsruhe Institute of Technology in 2012[26]. Similar to electrical wire bonding, which draws free-standing metal wires to connect metal contacts, photonic wire bonding leverages TPL technology to directly write polymer waveguide connections for optical couplings, as shown in Fig. 5a. In this scenario, multiple chips (or submodules) and fibers were placed and bonded to a carrier. The polymer waveguides were subsequently directly written using TPL to form interconnects between the optical channels on each submodule. The first photonic wire bonding (PWB) prototype consisted of two silicon-on-insulator (SOI) chips linked by SU-8 polymer waveguide connections. The PWB connections featured an average insertion loss of only 1.6 dB per bond in the C band and could transmit at an aggregate data rate of 5.25 Tbps[26].

Over a decade of progressive development since their initial demonstration, PWB has been empowered with increased writing speed, better precision, and reduced insertion loss. This technology has also been extended to multi-chip module packaging and fiber-to-chip coupling[110–114]. In one example, PWB was employed to link an InP laser chip, silicon modulator chip, silicon-arrayed waveguide grating chip, and single-mode fiber, all in a single package[110]. Notably, PWB enables adiabatic termination with component-specific designs to be implemented on different components. For example, an InP horizontal cavity surface-emitting laser and single-mode fiber interface adopted a rectangular linear taper to match the larger mode field diameter of the laser and minimize insertion losses. A minimum PWB insertion loss of 0.4 dB was reported between the laser and silicon chips when the laser emission spot was accurately aligned with the taper. Another example is a multi-core fiber (MCF) for waveguide connections, as shown in Fig. 5e[110]. To minimize the insertion loss, a double-inverse taper structure was employed to match the modes between the SOI and polymer waveguides. A shape-conversion section was incorporated to adiabatically transform the square cross-section of the waveguide to a circular shape and then expanded to match the fiber mode. This design resulted in a total insertion loss of 1.7 dB. More recently, a fully packaged optical communication engine using a hybrid multi-chip assembly was reported[111]. Based on the same configuration, this study further co-packaged another electrical RF interposer module to simultaneously control all Mach-Zender modulators (MZMs) as indicated in Fig. 5b. The average insertion loss of PWB over 100 waveguides was 0.75 ± 0.15 dB. In addition, the robustness of such a structure to thermal cycling was tested and confirmed in 225 cycles between −40 °C and 85 °C. The photonic transmitter engine could provide a 448 Gbps aggregated data rate over a 10 km distance when bonded with eight MZMs, eight lasers, and fibers. Furthermore, coherent communication is realized by bonding a four-channel quadrature (IQ) modulator to four lasers and four fibers. An aggregate data rate of 784 Gbps over 75 km has been experimentally demonstrated. In summary, PWB is a highly versatile packaging technique for a diverse range of multi-chip platforms[19,115,116].

Freeform microoptics

Freeform optics are ideally suited for optical coupling

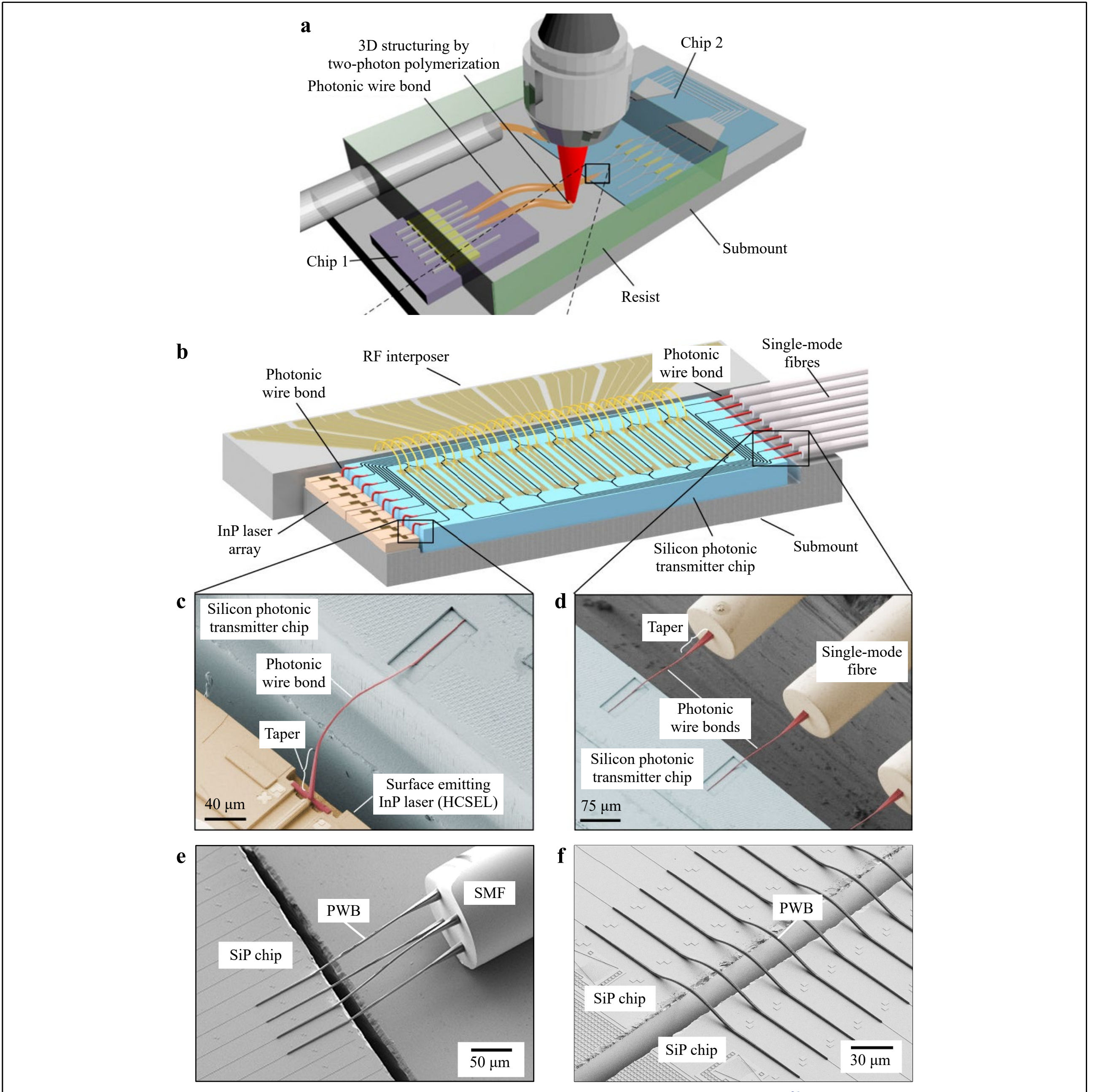

Fig. 5 Photonic wire bonding (PWB). **a** Schematic illustration of PWB, reprinted from Lindenmann et al.[26]. **b**–**d** Co-packaged hybrid multi-chip assembly module, reprinted from Blaicher et al.[111]. **e** and **f** Chip to multi-core fiber and chip-to-chip interconnects via PWB, respectively. Reprinted from Billah et al.[110].

elements owing to their capacity to sculpt light wavefronts. However, the widespread adoption of traditional bulk freeform optics has been hampered by complicated fabrication and integration procedures and high costs. Compared to simple spherical optics, freeform optics are often more sensitive to misalignment, and the resulting stringent assembly tolerance further negates the benefits of traditional bulk freeform optics. TPL presents a plausible route for producing freeform microoptics with high geometric fidelity and alignment precision. Therefore, they can be readily integrated with on-chip waveguide devices to create low-loss optical interfaces with other on-chip or off-chip components.

These freeform microoptical elements can be integrated into waveguides in two configurations. The first architecture involves the fabrication of an on-chip waveguide taper with the top cladding removed. A polymer waveguide section (typically defined by the TPL) was

subsequently overlaid on top of the taper. This composite waveguide structure enables the optical mode, initially confined in the on-chip waveguide, to adiabatically transition into the polymer waveguide. The polymer waveguide then funnels light toward the freeform microoptical element, which reshapes and redirects the optical mode to match that of the other components. The advantage of this approach is that the intermediate polymer waveguide seamlessly bridges the effective index difference between high-index-contrast on-chip waveguides and polymer-based freeform microoptics to minimize reflection and scattering losses. Moreover, the small numerical aperture (NA) of the polymer waveguides reduces the beam divergence upon exit, which considerably simplifies the optical coupler design[117]. Fig. 6 illustrates several coupler designs based on this configuration. In all cases, light is transferred into a polymer waveguide, which either directly mates with the fiber through a 3-D out-of-plane bend or couples with a TPL-printed microoptical element to direct the light toward the fiber[57,118,119]. A coupling loss of 1 dB was attained in the C band using a 3-D waveguide bend coupler, as shown in Fig. 6a[119]. Fig. 6b shows a coupler that combines a TIR mirror and concentrating spherical lens, which achieves a coupling loss of 3.1 dB at visible wavelengths[57]. In contrast to grating-based approaches, these are broadband couplers; for example, operation across both the visible and near-IR telecom bands in a single coupler has been demonstrated[118]. A conceptually analogous design is implemented for free-space-to-surface-guided mode coupling[120]. Applications of these free-form couplers include photonic computing[121,122], data communications[123,124], optical coherence tomography[125,126], quantum optics[127–129], and high-power laser physics[130].

An alternative configuration bypasses the cladding-removal step and directly integrates microoptics on the facet of the waveguide[132]. Because the backend-cladding stripping process is typically offered only as a custom add-on in photonic foundries, this configuration facilitates wafer-scale integration with standard foundry-processed PICs with minimal customization (the waveguide facets can be defined in a deep-trench etching step as part of the foundry process rather than during dicing). The avoidance of exposed waveguide cores also improves the ruggedness of the devices. Dietrich et al. demonstrated a wide variety of facet-attached microoptical beam-shaping elements for hybrid photonic multi-chip packaging[41]. The realized components ranged from single concentrating lenses and

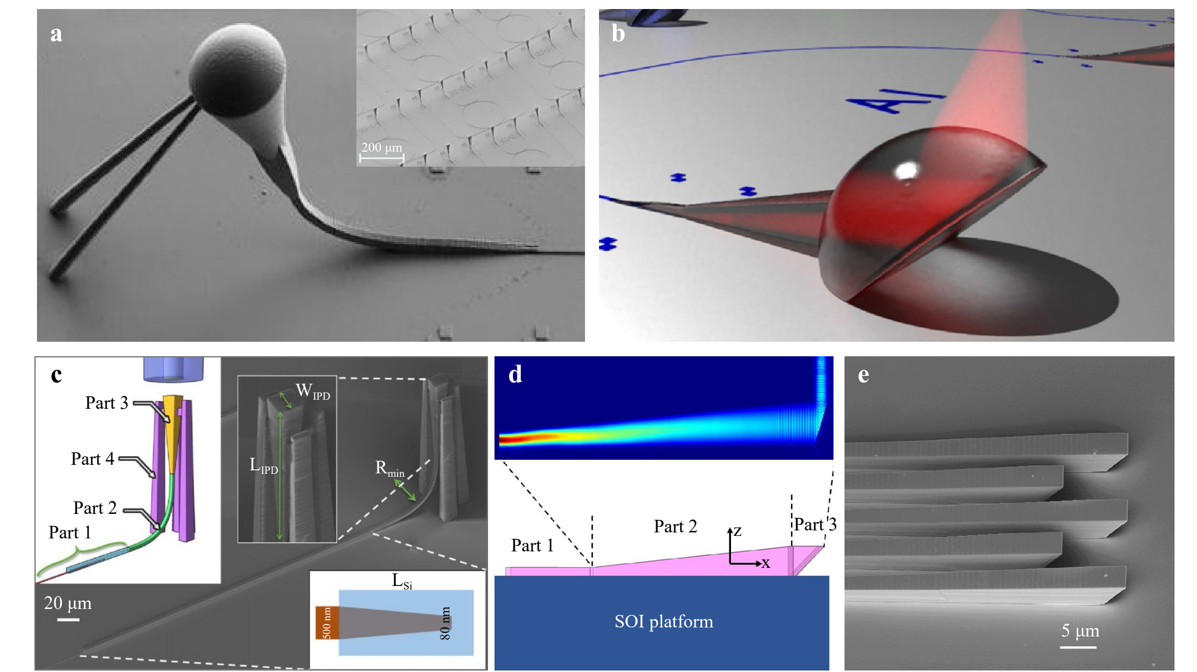

Fig. 6 Freeform microoptical couplers with a polymer waveguide-transition section. **a** SEM image of a waveguide to a fiber coupler.; inset: coupler array enabling high-density integration[118]. **b** Artistic view of a waveguide top attached TIR mirror. Reprinted from Gehring, H. et al.[57]. **c** Schematic drawing and corresponding SEM image of a waveguide-to-fiber vertical coupler, where a bent polymer waveguide directs the light toward a surface-normal propagation direction. Reprinted from Li, Y. et al.[50]. **d** Structure and FDTD simulation result of a waveguide-to-fiber TIR coupler; and **e** the SEM image arrays of the coupler. Here the TIR reflectors at the end of the polymer waveguides reflect the light upward toward the fiber. Reprinted from Luo et al.[131].

total internal reflective (TIR) mirrors to compound multi-lens assemblies (Fig. 7a), and their superior performance was validated. The concentrating lens/TIR mirror surfaces adopted a rotational/square symmetric polynomial of the eighth order, whose parameters were then optimized to achieve maximum coupling efficiency. The laser-to-fiber coupling loss using single free-form lenses was reduced to 0.6 dB, whereas the coupling loss from a vertical-cavity surface-emitting laser (VCSEL) to a TIR-mirror-integrated fiber was only 1.1 dB. The edge-emitting laser–chip-coupling loss was 2.5 dB with a 1-dB alignment tolerance of ± 2.5 μm. The repeatability of the TPL fabrication of these microoptical elements was also investigated with a device-to-device coupling loss variation of only 0.1 dB. These facet-attached microoptics are also applicable to the packaging of transceiver assemblies[133], Kerr comb sources[134,135], and lithium niobate on insulator modulators[135]. An interesting derivative of this concept is the printing of microoptics on the facets of a fiber array, which can be used as an optical probe for the wafer-level testing of edge-coupled devices that are normally only amenable to die-level characterization[136].

Yu et al. proposed microoptical reflectors as a 'universal' optical coupling platform, which they termed 'Optical Free-Form Couplers for High-density Integrated Photonics (OFFCHIP)'[137]. Their designs employed free-

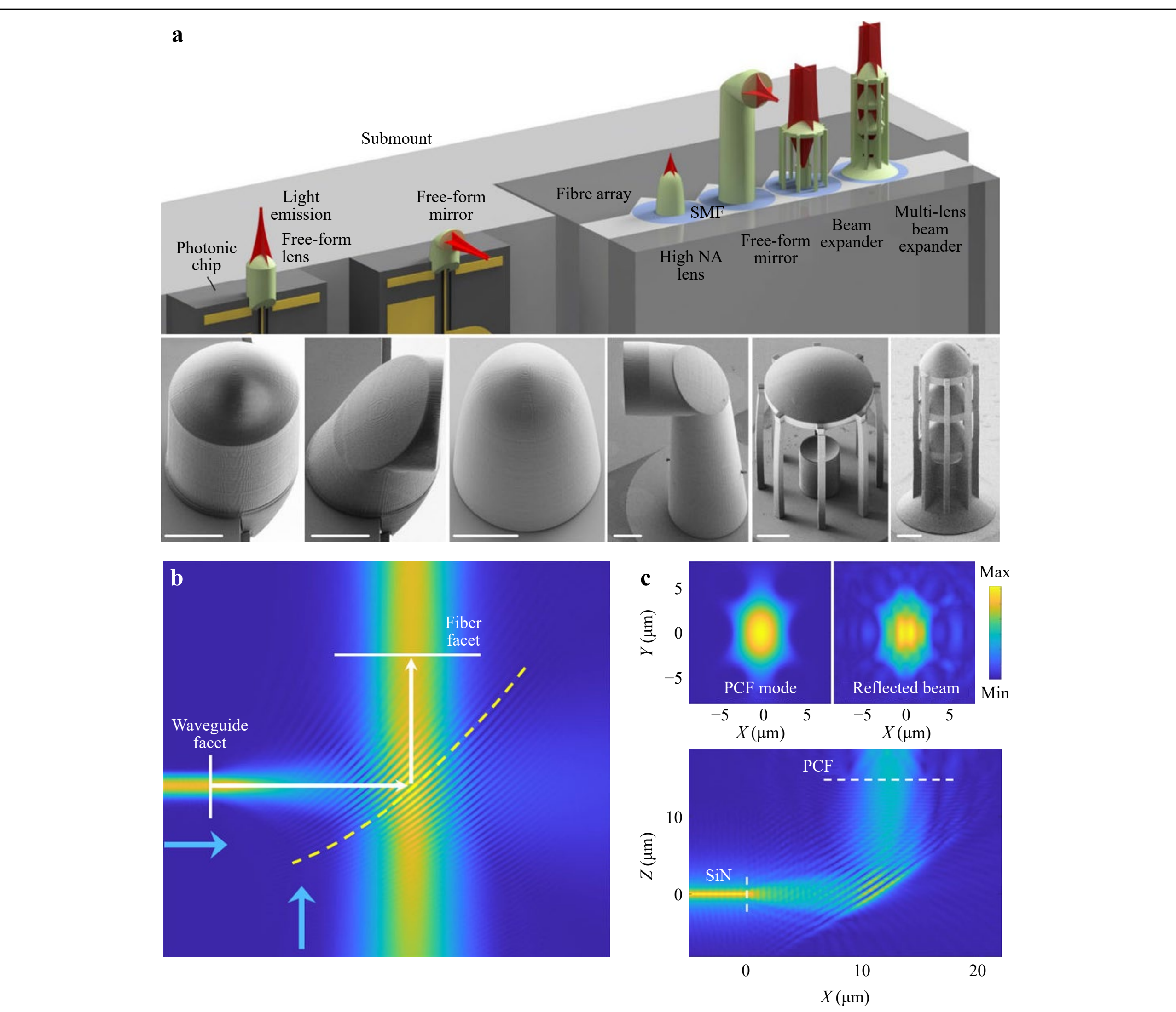

Fig. 7 Freeform facet-attached microoptics and their design methodology. **a** TPL-printed microoptic components for packaging, including freeform lenses, mirrors, and beam expanders. All scale bars are 20 μm. Adapted from Dietrich et al.[41]. **b** One-step deterministic design of freeform microoptics via a wavefront-based method. **c** Light coupling from a SiN waveguide into a photonic crystal fiber (PCF) via a facet-attached free-form coupler. **b** and **c** are adapted from Yu et al.[137].

form TIR mirrors to redirect and reshape optical waveguide modes to achieve low-loss, broadband surface-normal coupling[58,137]. Notably, they devised a novel approach that simplified the design of free-form elements from an otherwise iterative multi-parameter search-optimization process to a deterministic method involving only two full-wave simulations. The approach is illustrated in Fig. 7b, where a forward-propagating beam from the chip and a backward-propagating beam from the fiber create interference fringes in their overlapping region. Yu et al. demonstrated that these fringes represent loci of points satisfying the Fermat's principle, achieving a constant optical path length connecting the fiber and waveguide modes, which also yielded the optimal shape of the TIR reflector. Using this approach, the OFFCHIP platform can also be applied to coupling of light into devices with unconventional mode structures, such as photonic crystal fibers (Fig. 7c). The so-designed coupler[58] features a low insertion loss of 0.5 dB at 1550 nm wavelength and an ultra-broadband > 300 nm 1-dB bandwidth for coupling from a SiN waveguide to a single-mode fiber, with in-plane and out-of-plane 1-dB alignment tolerances of ± 2.2 and 20 μm, respectively. The OFFCHIP platform can also be adapted to coupling from chip-to-chip, chip-to-interposer, and chip-to-free space with tailored beam profiles[137].

Mechanical alignment structure

In addition to optical coupler printing, high spatial resolution and alignment accuracy qualify TPL as a versatile solution for the fabrication of micromechanical fixtures to assist in the passive alignment of optical components during packaging[138]. Wan et al. introduced the fiber-interconnect Si chip technology (FISCT) for fiber-to-chip packaging[139]. As depicted in Fig. 8a, it employs a carrier wafer with partial and through-etched pits to connect the fibers and silicon photonic chip. The partially etched pits are intended for self-alignment with the silicon host chip, whereas the through-holes are used for the bonding of 3-D printed fiber ferrules separately fabricated via TPL. During assembly, the carrier bonded with the ferrules was first placed on the photonic chip. The fibers were then inserted into these ferrules to complete the packaging. The fibers were self-aligned to the grating coupler, aided by a thermally reflowed photoresist dome structure on a photonic chip. Submicron placement accuracy was achieved using this method[140].

In another example, Gordillo et al. proposed a plug-and-play fiber-to-chip funnel-shaped connector module fabricated using TPL[141]. This consisted of a 20 μm aperture that was gradually reduced to 10 μm diameter to mechanically guide the fiber to align with the coupler center. Subsequently, the funnel was transformed into a solid-core polymer waveguide designed to match the fiber mode. Finally, the light was redirected via a TIR facet to impinge the normal surface onto a grating coupler. A schematic of this structure is shown in Fig. 8b. This coupler yielded an excess loss (relative to the coupling loss of the grating coupler) of only 0.05 dB at telecommunication wavelengths. TPL-fabricated connectors offer a reliable and robust assembly method for fiber-to-chip coupling. Although the bandwidth and total coupling loss were limited by the grating coupler in this study, combining these structures with low-loss broadband couplers will significantly improve the optical performance.

Industry adoption

The industrialization of a TPL places more stringent

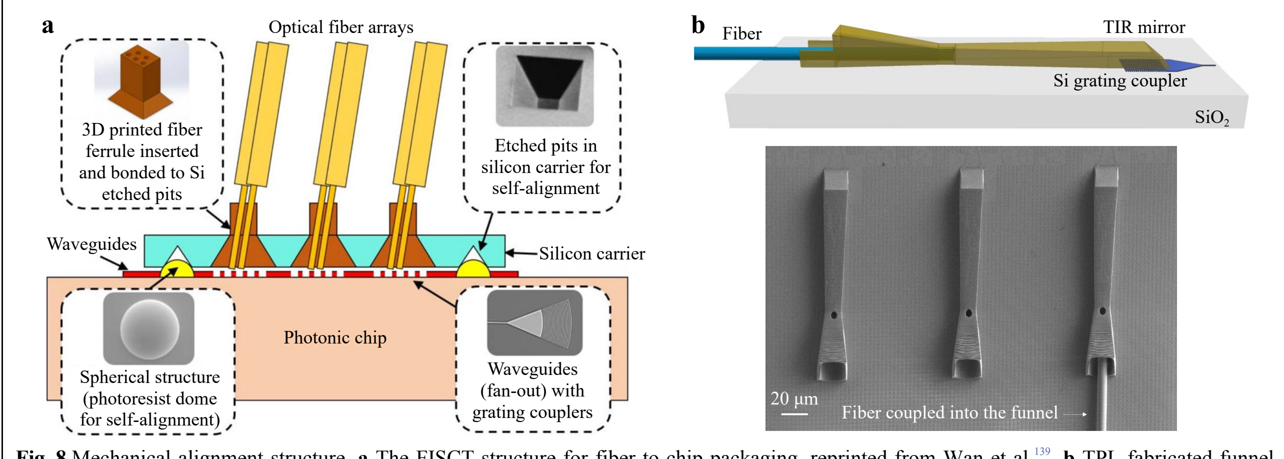

Fig. 8 Mechanical-alignment structure. **a** The FISCT structure for fiber-to-chip packaging, reprinted from Wan et al.[139]. **b** TPL-fabricated funnel structures for 'plug-and-play' fiber-to-chip connectors, adapted from Gordillo et al.[141].

requirements on its performance metrics. Several examples are:

1) Scalability and reliability: The first rigor of the industrial adoption of TP is its ability to consistently and reliably produce high-quality 3D structures, even when used for large-scale manufacturing.

2) Speed and precision: The cost of TPL-defined components scales directly with the printing time, among other factors. Therefore, it is essential for TPL to print structures quickly without sacrificing quality. High levels of precision and accuracy, down to the submicron scale, are required for complex 3-D structures, particularly in optical applications.

3) Ease of use: Industrialization also requires TPL tools to be easy to use and maintain. The tool should have a user-friendly interface and minimal maintenance requirements to reduce downtime and increase productivity.

Over the two decades since its initial debut, the effectivity of TPL has been validated, and several companies have already offered commercial off-the-shelf tools for TPL fabrication. Nanoscribe GmbH & Co. KG was the first to successfully commercialize TPL-based 3-D printing systems. Its latest product, Quantum X, uses a 250 mW, 780 nm femtosecond laser as the light source and offers up to 4096 level grayscale lithography capability to reduce the surface roughness to < 5 nm. The minimum feature size was 100 nm, determined using the focal spot size of the laser. The writer head scanner supports scan speeds up to 1.25 m/s when used in conjunction with a 5x magnification objective lens. The system specifies a 3-D alignment accuracy of less than 100 nm in-plane and 500 nm out-of-plane; the latter is achieved using the co-focal detection of markers. Heidelberg Instruments Mikrotechnik GmbH, in collaboration with Multiphoton Optics GmbH, launched MPO100 TPL system. The MPO100 tool is equipped with a 522 nm laser, which considerably expands the applicability of TPL polymers. Using a galvanoscanner, the tool can also scan at speeds up to 1 m/s with a 10x objective. The minimum feature size and surface roughness were specified as 100 and 10 nm, respectively. A unique feature of MPO100 is its stitching-free writing capability, which leverages simultaneous laser scanning and sample-stage movement. Compared to field-to-field writing, this continuous printing mode avoids possible discontinuities between fields. This is particularly useful for fabricating large connected structures with sizes bigger than those of a single writing field. UpNano GmbH is another company that focuses on TPL systems that feature high-power laser heads and large working distances. Their NanoOne 1000 model adopted a 780 nm and 90 fs pulse laser with an average power exceeding 1000 mW. The high power reduces the dwell time during writing, yielding a faster scan speed. In addition, it provides a vat mode for immersion lithography, where a vat with a specialty glass window protects the objective from the photoresist. Using the vat mode, NanoOne 1000 can fabricate structures up to 40 mm in height. Other companies offering TPL tools include Microlight3D, Laser NanoFab GmbH, and Innofocus Photonics Technology Pty., Ltd.

In addition to the aforementioned general-purpose TPL systems, Vanguard Automation GmbH has developed highly automated TPL tools that target photonic packaging applications. In addition to TPL printing, these systems can also performing automated dispensing of photoresist, development of exposed structures, and feature automated interface-detection functions using state-of-the-art machine vision tools.

Several companies and packaging houses, such as Vanguard Automation GmbH (Germany), Dream Photonics (Canada), and PhiX (Netherlands), offer custom TPL fabrication services. For PWB in a multi-chip

Table 2 TPL tool and photonic packaging service vendors

	Company	Website
Tool vendor	Nanoscribe GmbH & Co. KG	www.nanoscribe.com
	Vanguard Automation GmbH	www.vanguard-automation.com
	Multiphoton Optics GmbH	www.multiphoton.de
	Microlight3D	www.microlight3d.com
	UpNano GmbH	www.upnano.at
	Laser nanoFab GmbH	www.lasernanofab.com
	Innofocus Photonics Technology Pty Ltd	www.innofocus.com.au
Photonic packaging service provider	Dream Photonics Inc.	www.dreamphotonics.com
	PHIX Photonics Assembly	www.phix.com

assembly, predefined alignment markers must be patterned near the waveguide ends to be connected by PWB. The chips are mounted side-by-side on a carrier module with the waveguide ends facing each other. Subsequently, PWB can be used to connect the waveguides on the two chips. Mounts with V-grooves are employed for the fiber-to-chip PWB service. In addition to PWB, fabrication services for facet-attached microoptical lenses or reflectors based on customer-furnished designs are available.

Future trends

Although the latest advances discussed in this review have firmly positioned TPL as a high-performance and versatile solution for photonic packaging, innovations in several areas are warranted before TPL can become a mainstream packaging technology, as outlined below.

Fabrication throughput

High throughput is the linchpin for cost-effective volume production. The classical point-to-point TPL exposure scheme is time consuming and cannot compete with traditional packaging techniques. For example, each photonic wire bond requires tens or even hundreds of seconds to fabricate. In comparison, ~ 0.1 s per bond is typical for electrical wire bonding, which is generally not considered a high-throughput packaging technique. Several new writing schemes have been proposed to enhance the TPL throughput. The shell-and-scaffold writing scheme, with fine carving of only the shell, followed by fast coarse exposure of the core, considerably enhances the throughput of the TPL while maintaining the high-resolution advantage[142]. Projection-based light sheet exposure can be used to pattern complex structures layer-by-layer (Fig. 10b) instead of point-by-point (Fig. 10a), which can improve the TPL throughput by up to three orders of magnitude[143,144]. Multiple-beam parallel writing is another promising approach (Fig. 10c)[145–147]. For instance, nine beamlets generated from a diffractive optical element can be used for the parallel fabrication of large periodic arrays with submicron feature sizes[145]. An alternative solution to the throughput bottleneck is nanoimprinting or embossing for structure replication using TPL-fabricated masters as molds[117,118].

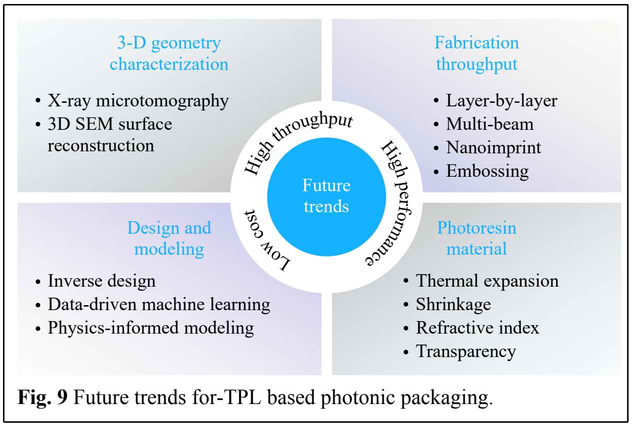

Fig. 9 Future trends for-TPL based photonic packaging.

Photoresin material

Photonic packaging applications require photoresins with improved thermo-mechanical properties and shape fidelity. First, polymers still pose challenges in terms of reliability and compatibility with photonic packages. Compared with the semiconductor and inorganic dielectric materials routinely used in PICs, many polymers are more susceptible to chemical degradation owing to thermal cycling, damp heat, or UV irradiation. Polymers typically have large thermal expansion coefficients (CTEs), compared to inorganic materials, which can cause mechanical failures such as delamination. 3-D structures made entirely of inorganic materials can be printed using hybrid organic-inorganic photoresins, followed by calcination (Section 2.1); however, the calcination step often requires high temperatures that exceed the packaging thermal budget and induces large shape distortions. Second, polymer-based photoresins typically exhibit 3%–5% volume shrinkage during cross-linking, which results in inevitable shape distortion. Although such

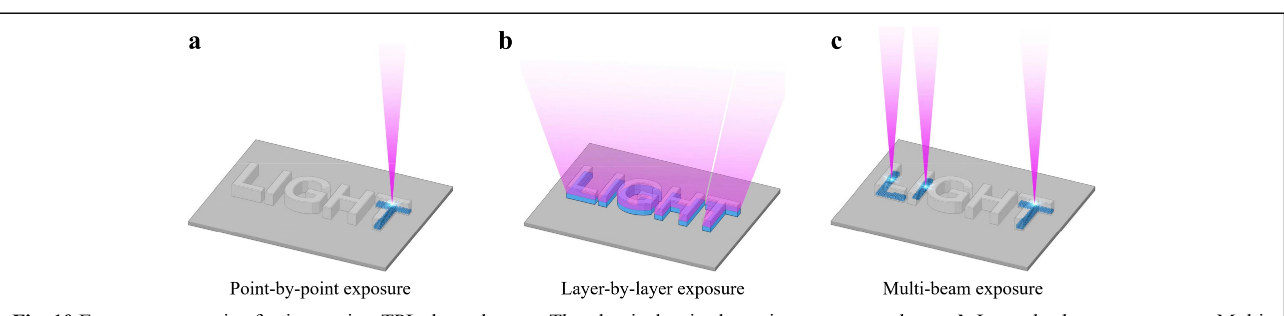

Fig. 10 Exposure strategies for improving TPL throughput. **a** The classical point-by-point exposure scheme. **b** Layer-by-layer exposure. **c** Multi-beam exposure.

distortions can be iteratively corrected or compensated using predictive techniques (discussed later), reduced shrinkage can significantly simplify the optimization process and shorten the design cycle. Finally, photoresins with a wide refractive-index range can significantly expand the accessible degrees of freedom for photonic designs. Doping with high-index nanoparticles is one method to increase the refractive index of resins. Shifting to photopolymer chemistries containing heavier elements such as sulfur may be another approach for extending the refractive index range[148].

Design and modeling

Because of the vast geometric degrees of freedom made available by the TPL technique, the design of these complex 3-D micro-structures presents another challenge. We also note that, unlike conventional freeform optics, which are customarily optimized with ray tracing, microoptical elements printed with TPL represent a unique length-scale regime in which ray optics meet wave optics. Therefore, novel design methods capable of handling large parameter sets of freeform microoptics in a computationally efficient manner, while accounting for the wave nature of light, are essential. The wavefront-based design approach outlined in Section 3.2 serves as an example. Coupling emerging inverse design and optimization algorithms with TPL fabrication of complex 3-D structures is another exciting area for future investigation[149].

Modeling the TPL process, which helps inform process optimization and enhances the shape fidelity of printed structures, is another important research frontier. Such models can be built on deterministic multiphysics simulations, such as the modeling of temperature and stress distribution during TPL fabrication or subsequent packaging processes[150]. When handling complex scenarios in which direct simulations prove difficult, data-driven machine learning is a complementary tool. Examples of its implementation include improving the geometric compliance of TPL-printed structures[151], enabling automated structural quality quantification[151], and developing predictive models for the constitutive relations of resin materials[150]. Harnessing physics-informed models may provide further insights into machine-learning techniques and expand their application to TPL process design and quality control.

3-D geometry characterization

The accurate and high-throughput characterizing of 3-D structure geometries is an important yet unresolved challenge for TPL-based photonic device fabrication. Conventional characterization methods for bulk freeform surfaces, such as white-light interferometry, are poorly adapted to microscale structures. Microscale surface metrology techniques such as profilometry or atomic force microscopy (AFM) are not applicable to surfaces with steep slopes or structures that are not fabricated on a planar substrate (e.g., facet-attached microoptics). Scanning electron microscopy (SEM) aided by an automated 3-D geometry reconstruction algorithm offers a potential solution for the high-throughput characterization of TPL-fabricated structures. Other advanced 3-D metrology characterization methods, exemplified by X-ray microtomography[152], are also of significant interest for this purpose.

Conclusions

Owing to its capability for high-resolution on-demand 3-D structure fabrication and precise placement, TPL is a promising solution for alleviating the photonic packaging bottleneck. TPL has been used to demonstrate optical coupling interfaces with exceptionally low optical loss, broadband operation, and enhanced alignment tolerance. 3-D printing of micromechanical self-alignment structures to aid in facile photonic assembly is another area in which TPL can play a pivotal role. As the community witnessed the increasing adoption of TPL by the photonics industry, we foresee that this trend will be expedited with further research and development efforts to boost TPL fabrication throughput while expanding the material repertoire as well as the design and characterization toolbox.

Acknowledgements

S. Y. and Q. D. acknowledge funding support from the National Key R&D Program of China 2021ZD0109904 and the Key Research Project of Zhejiang Lab No. 2022PH0AC03. C. R. M. acknowledges the funding support provided by the Fulbright Program.

Author details

[1]Zhejiang Laboratory, Hangzhou 311100, China. [2]Department of Materials Science and Engineering, Massachusetts Institute of Technology, Cambridge, MA 02139, USA. [3]Sao Carlos Institute of Physics, University of Sao Paulo, Sao Carlos, SP 13560-970, Brazil. [4]Materials Research Laboratory, Massachusetts Institute of Technology, Cambridge, MA 02139, USA

Conflict of interest

The authors declare no competing interests.

Received: 01 March 2023 Revised: 29 August 2023 Accepted: 31 August 2023
Accepted article preview online: 13 September 2023
Published online: 01 November 2023

References

1. Soref, R. Silicon photonics: a review of recent literature. *Silicon* **2**, 1-6

(2010).
2. Thylén, L. & Wosinski, L. Integrated photonics in the 21st century. *Photonics Research* **2**, 75-81 (2014).
3. Liang, D. & Bowers, J. E. Recent progress in heterogeneous III-V-on-silicon photonic integration. *Light:Advanced Manufacturing* **2**, 5 (2021).
4. Lin, H. T. et al. Mid-infrared integrated photonics on silicon: a perspective. *Nanophotonics* **7**, 393-420 (2017).
5. Wang, J. & Long, Y. On-chip silicon photonic signaling and processing: a review. *Science Bulletin* **63**, 1267-1310 (2018).
6. Li, N. X. et al. A progress review on solid-state LiDAR and nanophotonics-based LiDAR sensors. *Laser & Photonics Reviews* **16**, 2100511 (2022).
7. Passaro, V. M. N. et al. Recent advances in integrated photonic sensors. *Sensors* **12**, 15558-15598 (2012).
8. Shastri, B. J. et al. Photonics for artificial intelligence and neuromorphic computing. *Nature Photonics* **15**, 102-114 (2021).
9. Kita, D. M. et al. High-performance and scalable on-chip digital Fourier transform spectroscopy. *Nature Communications* **9**, 4405 (2018).
10. Pelucchi, E. et al. The potential and global outlook of integrated photonics for quantum technologies. *Nature Reviews Physics* **4**, 194-208 (2022).
11. Cheben, P. et al. Subwavelength integrated photonics. *Nature* **560**, 565-572 (2018).
12. Siew, S. Y. et al. Review of silicon photonics technology and platform development. *Journal of Lightwave Technology* **39**, 4374-4389 (2021).
13. Ranno, L. et al. Integrated photonics packaging: challenges and opportunities. *ACS Photonics* **9**, 3467-3485 (2022).
14. Carroll, L. et al. Photonic packaging: transforming silicon photonic integrated circuits into photonic devices. *Applied Sciences* **6**, 426 (2016).
15. Marchetti, R. et al. Coupling strategies for silicon photonics integrated chips [Invited]. *Photonics Research* **7**, 201-239 (2019).
16. Pavarelli, N. et al. Optical and electronic packaging processes for silicon photonic systems. *Journal of Lightwave Technology* **33**, 991-997 (2015).
17. Lee, J. S. et al. Meeting the electrical, optical, and thermal design challenges of photonic-packaging. *IEEE Journal of Selected Topics in Quantum Electronics* **22**, 8200209 (2016).
18. Li, L. et al. A fully-integrated flexible photonic platform for chip-to-chip optical interconnects. *Journal of Lightwave Technology* **31**, 4080-4086 (2013).
19. Nezami, M. S. et al. Packaging and interconnect considerations in neuromorphic photonic accelerators. *IEEE Journal of Selected Topics in Quantum Electronics* **29**, 6100311 (2023).
20. Mahajan, R. et al. Co-packaged photonics for high performance computing: status, challenges and opportunities. *Journal of Lightwave Technology* **40**, 379-392 (2022).
21. Kopp, C. et al. Silicon photonic circuits: On-CMOS integration, fiber optical coupling, and packaging. *IEEE Journal of Selected Topics in Quantum Electronics* **17**, 498-509 (2011).
22. Barwicz, T. et al. Automated, high-throughput photonic packaging. *Optical Fiber Technology* **44**, 24-35 (2018).
23. Zhao, Y., Lin, L. H. & Sun, H. B. On-chip optical interconnection based on two-photon polymerization (Invited). *Acta Photonica Sinica* **51**, 0851512 (2022).
24. Liu, S. F. *et al*. 3D laser nanoprinting of functional materials. *Advanced Functional Materials* 2211280,doi: 10.1002/adfm.202211280 (in the press).
25. Maruo, S., Nakamura, O. & Kawata, S. Three-dimensional microfabrication with two-photon-absorbed photopolymerization. *Optics Letters* **22**, 132-134 (1997).
26. Lindenmann, N. et al. Photonic wire bonding: a novel concept for chip-scale interconnects. *Optics Express* **20**, 17667-17677 (2012).
27. Adão, R. M. R. et al. Two-photon polymerization simulation and fabrication of 3D microprinted suspended waveguides for on-chip optical interconnects. *Optics Express* **30**, 9623-9642 (2022).
28. Lee, C. W. et al. Perpendicular coupling to in-plane photonics using arc waveguides fabricated via two-photon polymerization. *Applied Physics Letters* **100**, 171102 (2012).
29. Klein, S. et al. One-step waveguide and optical circuit writing in photopolymerizable materials processed by two-photon absorption. *Applied Physics Letters* **86**, 211118 (2005).
30. Schmidt, V. et al. Two-photon 3D lithography: A versatile fabrication method for complex 3D shapes and optical interconnects within the scope of innovative industrial applications. *Journal of Laser Micro/Nanoengineering* **2**, 170-177 (2007).
31. Ishihara, J. et al. Fabrication of three-dimensional calixarene polymer waveguides using two-photon assisted polymerization. *Applied Physics Letters* **90**, 033511 (2007).
32. Schmid, G. et al. Gbit/s transmission via two-photon-absorption-inscribed optical waveguides on printed circuit boards. *Electronics Letters* **45**, 219-221 (2009).
33. Seidel, A. et al. Nanoimprinting of dielectric loaded surface-plasmon-polariton waveguides using masters fabricated by 2-photon polymerization technique. *Journal of the Optical Society of America B* **26**, 810-812 (2009).
34. Serbin, J. & Gu, M. Superprism phenomena in waveguide-coupled woodpile structures fabricated by two-photon polymerization. *Optics Express* **14**, 3563-3568 (2006).
35. Gonzalez-Hernandez, D. et al. Micro-optics 3D printed via multi-photon laser lithography. *Advanced Optical Materials* **11**, 2201701 (2023).
36. Moscoso-Martir, A. et al. Hybrid silicon photonics flip-chip laser integration with vertical self-alignment. 2017 Conference on Lasers and Electro-Optics Pacific Rim (CLEO-PR). Singapore: IEEE, 2017, 1-4.
37. Theurer, M. et al. Flip-chip integration of InP to SiN photonic integrated circuits. *Journal of Lightwave Technology* **38**, 2630-2636 (2020).
38. Shimizu, T. et al. High density hybrid integrated light source with a laser diode array on a silicon optical waveguide platform for inter-chip optical interconnection. 8th IEEE International Conference on Group IV Photonics. London: IEEE, 2011, 181-183.
39. Schmid, M. D. et al. 3D direct laser writing of highly absorptive photoresist for miniature optical apertures. *Advanced Functional Materials*, 2211159 (in the press).
40. Schmid, M. et al. 3D printed hybrid refractive/diffractive achromat and apochromat for the visible wavelength range. *Optics Letters* **46**, 2485-2488 (2021).
41. Dietrich, P. I. et al. In situ 3D nanoprinting of free-form coupling elements for hybrid photonic integration. *Nature Photonics* **12**, 241-247 (2018).
42. Weiß, T. et al. Two-photon polymerization of biocompatible photopolymers for microstructured 3D biointerfaces. *Advanced Engineering Materials* **13**, B264-B273 (2011).
43. Gittard, S. D. et al. Fabrication of microscale medical devices by two-photon polymerization with multiple foci via a spatial light modulator. *Biomedical Optics Express* **2**, 3167-3178 (2011).
44. O' Halloran, S. et al. Two-photon polymerization: fundamentals, materials, and chemical modification strategies. *Advanced Science* **10**, 2204072 (2023).
45. Otuka, A. J. G. et al. Two-photon polymerization: functionalized microstructures, micro-resonators, and bio-scaffolds. *Polymers* **13**,

1994 (2021).

46. Vyatskikh, A. et al. Additive manufacturing of 3D nano-architected metals. *Nature Communications* **9**, 593 (2018).
47. Portela, C. M. et al. Supersonic impact resilience of nanoarchitected carbon. *Nature Materials* **20**, 1491-1497 (2021).
48. Sharipova, M. I. et al. Effect of pyrolysis on microstructures made of various photoresists by two-photon polymerization: comparative study. *Optical Materials Express* **11**, 371-384 (2021).
49. Hohmann, J. K. et al. Three-dimensional μ-printing: an enabling technology. *Advanced Optical Materials* **3**, 1488-1507 (2015).
50. Li, Y. et al. UV to NIR optical properties of IP-Dip, IP-L, and IP-S after two-photon polymerization determined by spectroscopic ellipsometry. *Optical Materials Express* **9**, 4318-4328 (2019).
51. Bauer, J. et al. Thermal post-curing as an efficient strategy to eliminate process parameter sensitivity in the mechanical properties of two-photon polymerized materials. *Optics Express* **28**, 20362-20371 (2020).
52. Rohbeck, N. et al. Effect of high strain rates and temperature on the micromechanical properties of 3D-printed polymer structures made by two-photon lithography. *Materials & Design* **195**, 108977 (2020).
53. Wang, S. H. et al. Sub-10-nm suspended nano-web formation by direct laser writing. *Nano Futures* **2**, 025006 (2018).
54. Liu, Y. J. et al. Structural color three-dimensional printing by shrinking photonic crystals. *Nature Communications* **10**, 4340 (2019).
55. Schmid, M., Ludescher, D. & Giessen, H. Optical properties of photoresists for femtosecond 3D printing: refractive index, extinction, luminescence-dose dependence, aging, heat treatment and comparison between 1-photon and 2-photon exposure. *Optical Materials Express* **9**, 4564-4577 (2019).
56. Rad, Z. F., Prewett, P. D. & Davies, G. J. High-resolution two-photon polymerization: the most versatile technique for the fabrication of microneedle arrays. *Microsystems & Nanoengineering* **7**, 71 (2021).
57. Gehring, H. et al. Broadband out-of-plane coupling at visible wavelengths. *Optics Letters* **44**, 5089-5092 (2019).
58. Yu, S. L. et al. Free-form micro-optics enabling ultra-broadband low-loss off-chip coupling. *Laser & Photonics Reviews* **17**, 2200025 (2023).
59. Gissibl, T. et al. Sub-micrometre accurate free-form optics by three-dimensional printing on single-mode fibres. *Nature Communications* **7**, 11763 (2016).
60. Hot Lithography® – UpNano – high-resolution 3D printing. at https://www.upnano.at/hot-lithography/.
61. Bunea, A. I. et al. Micro 3D printing by two-photon polymerization: configurations and parameters for the nanoscribe system. *Micro* **1**, 164-180 (2021).
62. Hasegawa, T. , Oishi, K. & Maruo, S. Three-dimensional microstructuring of PDMS by two-photon microstereolithography. 2006 IEEE International Symposium on MicroNanoMechanical and Human Science. Nagoya: IEEE, 2006, 1-4, doi: 10.1109/MHS.2006.320261.
63. Panusa, G. et al. Fabrication of sub-micron polymer waveguides through two-photon polymerization in polydimethylsiloxane. *Polymers* **12**, 2485 (2020).
64. Murata, N. & Nakamura, K. UV-curable adhesives for optical communications. *The Journal of Adhesion* **35**, 251-267 (1991).
65. Lorenz, H. et al. High-aspect-ratio, ultrathick, negative-tone near-UV photoresist and its applications for MEMS. *Sensors and Actuators A:Physical* **64**, 33-39 (1998).
66. Chen, M. H. et al. Low shrinkage light curable nanocomposite for dental restorative material. *Dental Materials* **22**, 138-145 (2006).
67. Teh, W. H. et al. Effect of low numerical-aperture femtosecond two-photon absorption on (SU-8) resist for ultrahigh-aspect-ratio microstereolithography. *Journal of Applied Physics* **97**, 054907 (2005).
68. Tottori, S. et al. Magnetic helical micromachines: fabrication, controlled swimming, and cargo transport. *Advanced Materials* **24**, 811-816 (2012).
69. Kumi, G. et al. High-speed multiphoton absorption polymerization: fabrication of microfluidic channels with arbitrary cross-sections and high aspect ratios. *Lab on a Chip* **10**, 1057-1060 (2010).
70. Streppel, U. et al. Formation of micro-optical structures by self-writing processes in photosensitive polymers. *Applied Optics* **42**, 3570-3579 (2003).
71. Maydykovskiy, A. I. et al. Two-photon laser lithography of active microcavity structures. *JETP Letters* **115**, 261-266 (2022).
72. Zuo, H. J. et al. Low loss, flexible single-mode polymer photonics. *Optics Express* **27**, 11152-11159 (2019).
73. Gonzalez-Hernandez, D. et al. Laser 3D printing of inorganic free-form micro-optics. *Photonics* **8**, 577 (2021).
74. Kotz, F. et al. Two-photon polymerization of nanocomposites for the fabrication of transparent fused silica glass microstructures. *Advanced Materials* **33**, 2006341 (2021).
75. Kotz, F. et al. Liquid glass: a facile soft replication method for structuring glass. *Advanced Materials* **28**, 4646-4650 (2016).
76. Kotz, F. et al. Three-dimensional printing of transparent fused silica glass. *Nature* **544**, 337-339 (2017).
77. Suter, M. et al. Superparamagnetic microrobots: fabrication by two-photon polymerization and biocompatibility. *Biomedical Microdevices* **15**, 997-1003 (2013).
78. Masui, K. et al. Laser fabrication of Au nanorod aggregates microstructures assisted by two-photon polymerization. *Optics Express* **19**, 22786-22796 (2011).
79. Marino, A. et al. Two-photon lithography of 3D nanocomposite piezoelectric scaffolds for cell stimulation. *ACS Applied Materials & Interfaces* **7**, 25574-25579 (2015).
80. Xing, J. F., Zheng, M. L. & Duan, X. M. Two-photon polymerization microfabrication of hydrogels: an advanced 3D printing technology for tissue engineering and drug delivery. *Chemical Society Reviews* **44**, 5031-5039 (2015).
81. Song, J. X. et al. From simple to architecturally complex hydrogel scaffolds for cell and tissue engineering applications: opportunities presented by two-photon polymerization. *Advanced Healthcare Materials* **9**, 1901217 (2020).
82. Xu, Y. A. et al. Deep ultraviolet hydrogel based on 2D cobalt-doped titanate. *Light:Science & Applications* **12**, 1 (2023).
83. Ding, B. F. et al. A 2D material–based transparent hydrogel with engineerable interference colours. *Nature Communications* **13**, 1212 (2022).
84. Saccone, M. A. et al. Additive manufacturing of micro-architected metals via hydrogel infusion. *Nature* **612**, 685-690 (2022).
85. Oran, D. et al. 3D nanofabrication by volumetric deposition and controlled shrinkage of patterned scaffolds. *Science* **362**, 1281-1285 (2018).
86. Lu, X. M. et al. Hierarchically porous monoliths prepared via sol–gel process accompanied by spinodal decomposition. *Journal of Sol-Gel Science and Technology* **95**, 530-550 (2020).
87. Schwarz, C. M. et al. Multi-photon lithography of 3D micro-structures in As_2S_3 and $Ge_5(As_2Se_3)95$ chalcogenide glasses. Proceedings of the SPIE 9759, Advanced Fabrication Technologies for Micro/Nano Optics and Photonics IX. San Francisco: SPIE, 2016, 975916.
88. Wong, S. et al. Direct laser writing of three- dimensional photonic crystals with a complete photonic bandgap in chalcogenide glasses. *Advanced Materials* **18**, 265-269 (2006).
89. Cumming, B. P. et al. Adaptive optics enhanced direct laser writing of high refractive index gyroid photonic crystals in chalcogenide glass. *Optics Express* **22**, 689-698 (2014).

90. Schwarz, C. M. et al. Structurally and morphologically engineered chalcogenide materials for optical and photonic devices. *Journal of Optical Microsystems* **1**, 013502 (2021).
91. Zhang, Y. S. et al. Two-photon 3D printing in metal–organic framework single crystals. *Small* **18**, 2200514 (2022).
92. Yu, J. C. et al. Two-photon responsive metal–organic framework. *Journal of the American Chemical Society* **137**, 4026-4029 (2015).
93. Gissibl, T. et al. Two-photon direct laser writing of ultracompact multi-lens objectives. *Nature Photonics* **10**, 554-560 (2016).
94. Liu, Y. et al. Deformation behavior of foam laser targets fabricated by two-photon polymerization. *Nanomaterials* **8**, 498 (2018).
95. Rosenbohm, J. et al. A multi-material platform for imaging of single cell-cell junctions under tensile load fabricated with two-photon polymerization. *Biomedical Microdevices* **24**, 33 (2022).
96. Zhang, X. N. et al. Complex refractive indices measurements of polymers in visible and near-infrared bands. *Applied Optics* **59**, 2337 (2020).
97. Malitson, I. H. Interspecimen comparison of the refractive index of fused silica. *Journal of the Optical Society of America* **55**, 1205 (1965).
98. Zhou, X. Q., Hou, Y. H. & Lin, J. Q. A review on the processing accuracy of two-photon polymerization. *AIP Advances* **5**, 030701 (2015).
99. Tanaka, T., Sun, H. B. & Kawata, S. Rapid sub-diffraction-limit laser micro/nanoprocessing in a threshold material system. *Applied Physics Letters* **80**, 312-314 (2002).
100. Guo, R. et al. Micro lens fabrication by means of femtosecond two photon photopolymerization. *Optics Express* **14**, 810-816 (2006).
101. Park, S. H. et al. Subregional slicing method to increase three-dimensional nanofabrication efficiency in two-photon polymerization. *Applied Physics Letters* **87**, 154108 (2005).
102. Wu, D. et al. High numerical aperture microlens arrays of close packing. *Applied Physics Letters* **97**, 31109 (2010).
103. Aderneuer, T., Fernández, O. & Ferrini, R. Two-photon grayscale lithography for free-form micro-optical arrays. *Optics Express* **29**, 39511-39520 (2021).
104. Wang, H. et al. Toward near-perfect diffractive optical elements via nanoscale 3D printing. *ACS Nano* **14**, 10452-10461 (2020).
105. Wollhofen, R. et al. 120 nm resolution and 55 nm structure size in STED-lithography. *Optics Express* **21**, 10831-10840 (2013).
106. He, M. F. et al. 3D sub-diffraction printing by multicolor photoinhibition lithography: from optics to chemistry. *Laser & Photonics Reviews* **16**, 2100229 (2022).
107. He, M. F. et al. Single-color peripheral photoinhibition lithography of nanophotonic structures. *PhotoniX* **3**, 25 (2022).
108. Yang, D. Y. et al. Ultraprecise microreproduction of a three-dimensional artistic sculpture by multipath scanning method in two-photon photopolymerization. *Applied Physics Letters* **90**, 013113 (2007).
109. Chidambaram, N. et al. Selective surface smoothening of polymer microlenses by depth confined softening. *Advanced Materials Technologies* **2**, 1700018 (2017).
110. Billah, M. R. et al. Hybrid integration of silicon photonics circuits and InP lasers by photonic wire bonding. *Optica* **5**, 876-883 (2018).
111. Blaicher, M. et al. Hybrid multi-chip assembly of optical communication engines by in situ 3D nano-lithography. *Light:Science & Applications* **9**, 71 (2020).
112. Lindenmann, N. et al. Connecting silicon photonic circuits to multicore fibers by photonic wire bonding. *Journal of Lightwave Technology* **33**, 755-760 (2015).
113. Gečys, P. et al. Ripple formation by femtosecond laser pulses for enhanced absorptance of stainless steel. *Journal of Laser Micro/Nanoengineering* **10**, 129-133 (2015).
114. Xu, Y. L. et al. Hybrid external-cavity lasers (ECL) using photonic wire bonds as coupling elements. *Scientific Reports* **11**, 16426 (2021).
115. Luan, E. X. et al. Towards a high-density photonic tensor core enabled by intensity-modulated microrings and photonic wire bonding. *Scientific Reports* **13**, 1260 (2023).
116. Schumann, M. et al. Hybrid 2D–3D optical devices for integrated optics by direct laser writing. *Light:Science & Applications* **3**, e175 (2014).
117. Yu, S. L. et al. Compact and fabrication-tolerant waveguide bends based on quadratic reflectors. *Journal of Lightwave Technology* **38**, 4368-4373 (2020).
118. Gehring, H. et al. Low-loss fiber-to-chip couplers with ultrawide optical bandwidth. *APL Photonics* **4**, 10801 (2019).
119. Luo, H. Z. et al. Low-loss and broadband fiber-to-chip coupler by 3D fabrication on a silicon photonic platform. *Optics Letters* **45**, 1236-1239 (2020).
120. Safronov, K. R. et al. Miniature Otto prism coupler for integrated photonics. *Laser & Photonics Reviews* **16**, 2100542 (2022).
121. Feldmann, J. et al. Parallel convolutional processing using an integrated photonic tensor core. *Nature* **589**, 52-58 (2021).
122. Brückerhoff-Plückelmann, F. et al. Broadband photonic tensor core with integrated ultra-low crosstalk wavelength multiplexers. *Nanophotonics* **11**, 4063-4072 (2022).
123. Yu, S. L. et al. Seamless hybrid-integrated interconnect NEtwork (SHINE). 2019 Optical Fiber Communications Conference and Exhibition. San Diego: IEEE, 2019, 1-3. doi:10.1364/OFC.2019.M4D.5.
124. Wang, X. X. et al. Design of hybrid plasmonic multi-quantum-well electro-reflective modulators towards <100 fJ/bit photonic links. *IEEE Journal of Selected Topics in Quantum Electronics* **27**, 3400108 (2021).
125. Schneider, S. et al. Optical coherence tomography system mass-producible on a silicon photonic chip. *Optics Express* **24**, 1573-1586 (2016).
126. Zvagelsky, R. et al. Towards *in-situ* diagnostics of multi-photon 3D laser printing using optical coherence tomography. *Light:Advanced Manufacturing* **3**, 466-480 (2022).
127. Eich, A. et al. Single-photon emission from individual nanophotonic-integrated colloidal quantum dots. *ACS Photonics* **9**, 551-558 (2022).
128. Preuß, J. A. et al. Low-divergence hBN single-photon source with a 3D-printed low-fluorescence elliptical polymer microlens. *Nano Letters* **23**, 407-413 (2023).
129. Terhaar, R. et al. Ultrafast quantum key distribution using fully parallelized quantum channels. *Optics Express* **31**, 2675-2688 (2023).
130. Wiste, T. et al. Additive manufactured foam targets for experiments on high-power laser–matter interaction. *Journal of Applied Physics* **133**, 043101 (2023).
131. Luo, H. Z. et al. Efficient four-way vertical coupler array for chip-scale space-division-multiplexing applications. *Optics Letters* **46**, 4324-4327 (2021).
132. Xu, Y. L. et al. 3D-printed facet-attached microlenses for advanced photonic system assembly. *Light: Advanced Manufacturing* **4**, 3 (2023).
133. Maier, P. et al. 3D-printed facet-attached optical elements for connecting VCSEL and photodiodes to fiber arrays and multi-core fibers. *Optics Express* **30**, 46602-46625 (2022).
134. Maier, P. et al. Sub-kHz-linewidth external-cavity laser (ECL) with Si_3N_4 resonator used as a tunable pump for a Kerr frequency comb. *Journal of Lightwave Technology* **41**, 3479-3490 (2023).
135. Chen, L. F. , Luo, H. Z. & Cai, X. L. 3D micro lenses for efficient edge coupling by two-photon lithography. Conference on Lasers and Electro-Optics. San Jose: OSA, 2021, doi:10.1364/CLEO_SI. 2021.SM4C.6.
136. Trappen, M. et al. 3D-printed optical probes for wafer-level testing of photonic integrated circuits. *Optics Express* **28**, 37996-38007 (2020).
137. Yu, S. L. et al. Optical free-form couplers for high-density integrated

photonics (OFFCHIP): a universal optical interface. *Journal of Lightwave Technology* **38**, 3358-3365 (2020).
138. Nair, S. P. et al. 3D printed fiber sockets for plug and play micro-optics. *International Journal of Extreme Manufacturing* **3**, 015301 (2021).
139. Wan, C. S. et al. Fiber-interconnect silicon chiplet technology for self-aligned fiber-to-chip assembly. *IEEE Photonics Technology Letters* **31**, 1311-1314 (2019).
140. Yu, S. T., Gaylord, T. K. & Bakir, M. S. Fiber-array-to-chip interconnections with sub-micron placement accuracy via self-aligning chiplets. *IEEE Photonics Technology Letters* **34**, 1023-1025 (2022).
141. Gordillo, O. A. J. et al. Plug-and-play fiber to waveguide connector. *Optics Express* **27**, 20305-20310 (2019).
142. Trautmann, A. et al. Scaffolds in a shell–a new approach combining one-photon and two-photon polymerization. *Optics Express* **26**, 29659-29668 (2018).
143. Saha, S. K. et al. Scalable submicrometer additive manufacturing. *Science* **366**, 105-109 (2019).
144. Hahn, V. et al. Light-sheet 3D microprinting via two-colour two-step absorption. *Nature Photonics* **16**, 784-791 (2022).
145. Maibohm, C. et al. Multi-beam two-photon polymerization for fast large area 3D periodic structure fabrication for bioapplications. *Scientific Reports* **10**, 8740 (2020).
146. Pisanello, M. et al. An open source three-mirror laser scanning holographic two-photon lithography system. *PLoS One* **17**, e0265678 (2022).
147. Obata, K. et al. Multi-focus two-photon polymerization technique based on individually controlled phase modulation. *Optics Express* **18**, 17193-17200 (2010).
148. Kleine, T. S. et al. 100th Anniversary of macromolecular science viewpoint: high refractive index polymers from elemental sulfur for infrared thermal imaging and optics. *ACS Macro Letters* **9**, 245-259 (2020).
149. Roberts, G. et al. 3D-patterned inverse-designed mid-infrared metaoptics. *Nature Communications* **14**, 2768 (2023).
150. Diamantopoulou, M., Karathanasopoulos, N. & Mohr, D. Stress-strain response of polymers made through two-photon lithography: Micro-scale experiments and neural network modeling. *Additive Manufacturing* **47**, 102266 (2021).
151. Yang, Y. H. et al. Machine-learning-enabled geometric compliance improvement in two-photon lithography without hardware modifications. *Journal of Manufacturing Processes* **76**, 841-849 (2022).
152. Landis, E. N. & Keane, D. T. X-ray microtomography. *Materials Characterization* **61**, 1305-1316 (2010).